SEMARAK ILMU PUBLISHING

Journal of Advanced Research in Applied Mechanics

Journal homepage:
https://semarakilmu.com.my/journals/index.php/appl_mech/index
ISSN: 2289-7895

Surface Refinement of Aluminium Oxide by Carbon-Based Reinforcement

Noor Ayuma Mat Tahir[1], Shahira Liza Kamis[1,*], Yazid Yaakob[2], Nur Afieqah Md Ghazazi[1]

[1] Malaysia–Japan International Institute of Technology, Universiti Teknologi Malaysia, Jalan Sultan Yahya Petra, 54100 Kuala Lumpur, Malaysia
[2] Department of Physics, Faculty of Science, Universiti Putra Malaysia, 43400 Serdang, Selangor, Malaysia

ARTICLE INFO

Article history:
Received 20 January 2023
Received in revised form 18 March 2023
Accepted 26 March 2023
Available online 14 April 2023

Keywords:
Composite coating; carbon reinforcement; hard anodizing; anodic oxide

ABSTRACT

This paper clarifies the surface difference and tribological performance of anodic oxide coating reinforced with three different carbon-based sources. With the rising age of oxide coating as one of the strongest metal surface protectors, modification and improvement of this coating have been rapidly explored, including reinforcing carbon-based materials. The lack of literature on how the correlation between the particles' size improves the surface condition and its tribological properties opens up the gap in expanding this coating's potential. In this study, aluminium alloy AA2017 has been chosen as the substrate to be anodized with three different carbon sources: micro-sized graphite, nano-sized graphite, and graphite plate. With a constant 2A current on the DC power supply, the substrate was anodized for 60 minutes in a 20% sulphuric acid electrolyte. The finding shows that the anodic oxide with nano-sized graphite produces the highest hardness surface with almost 50% improvement compared to the unreinforced anodic oxide coating with no visible micro-cracks on the surface observed. Tribologically, the anodic oxide reinforced with micro-sized graphite produced the lowest coefficient of friction and wear rate at 0.4 and 1.25x10-5 mm3/Nm, respectively. The wear track image shows traces of debris that are different for each type of anodic coating that might be influenced by the surface roughness and hardness of the coating.

1. Introduction

With the endless properties that could be provided by its combinations, aluminium alloy (AA) is one of the most used alloys on earth, where the AA2XXX series are often used in machinery, automotive, aircraft, and aerospace structures [1]. With copper as one of its main elements, the AA2XXX is a heat-treatable alloy with fair workability and corrosion resistance relative to its weight. Although this alloy is rather challenging to anodize, there is plenty of research focusing on improving the properties of this alloy to expand its potential applications due to its unique properties.

After decades of research, porous anodic alumina has emerged as one of the most widely used templates for forming new functional ordered nanostructures made of metal, inorganic, and polymer materials. These nanostructures have shown remarkable optic, electric, and magnetic properties [2].

* *Corresponding author.*
E-mail address: shahiraliza@utm.my

https://doi.org/10.37934/aram.105.1.2840

The typical fabrication of porous anodic alumina is hard anodizing. Hard anodizing is an emerging anodizing method that can be manufactured by using strong acids such as sulphuric, oxalic, and phosphoric acid [3–6]. As literally named by hard anodizing, the oxide coating produced by this anodizing method has a higher hardness and growth rate than the typical mild anodizing method. Unfortunately, oxide layers do not adhere to all alloys in the same way. Alloys with high copper or silicon concentrations typically have porous and relatively soft coatings.

Recently, it was discovered that the anodic oxide layers' porosity was useful for tribological applications because it served as a lubricant reservoir, improving friction and wear performances. It was claimed that the anodic oxide coating of aluminium alloys is synergistic with surface micro-texturing technology. Unfortunately, no significant study has been able to prove this claim yet systematically. In fact, it was found that significant surface roughness characteristics (pore conditions) have an adverse impact on the ability of an oil film to develop and decrease friction. In actuality, compared to the flat and micro-textured specimens, the anodizing micro-textured samples exhibit a higher oil-lubricated friction coefficient [7].

Throughout the past few years, the majority of researchers have concentrated on creating composite coatings incorporating different additives, such as Silicone Carbide (SiC), Silicone Dioxide (SiO_2), hydroxyapatite (HA), fly ash (FA), carbon nano-tubes (CNT), graphene, and graphene oxide (GO), in an effort to improve the wear and electrochemical corrosion resistances. The outcomes have demonstrated that the anodic oxide composite coatings offer very effective protection where entrapping hard particles in the coating often improves the hardness and has a beneficial impact on wear resistance [6,8–14].

To strengthen the surface condition, previous studies have added reinforcement such as highly dispersed polytetrafluoroethylene, polymethyltrimethoxysilane, and hydroxyapatite particles during Plasma Electrolytic Oxidation (PEO) on magnesium (Mg) or Titanium (Ti) alloy and found that the composite coating displayed improved wear and corrosion resistances [15–17]. Additionally, self-lubricating substances, including graphite, graphene, and molybdenum disulfide (MoS_2), have been used to enhance the antifriction qualities of PEO coatings on Mg alloys [12,18–25]. A superior self-lubricating and corrosion-inhibiting material for metal substrates, graphene oxide (GO) has recently shown growing signs of potential for use [13,26–28].

Despite the intense interest in improving the anodic oxide coating, there are gaps in further research to determine how these hard particles affect anodic coatings' ability to adsorb within the coating and its ability to resist wear and friction. Besides that, there is a limited number of works of literature that have focused on the wear characteristics of anodic aluminium oxide coating in a dry (non-lubricated) environment. It is considerably more difficult to come across a publication that examined the dry sliding behavior of hard anodized-anodic aluminium oxide coating under low-range load (1N).

2. Methodology

2.1 Sample Preparation

The substrate selected in this study is an aluminium alloy (AA2017) with the properties shown in Table 1 (received from the manufacturer). The substrate was cut into Ø25mm with 4mm thickness and Ø4mm hole, as shown in Figure 1. The surface was then ground and polished until it reached average surface roughness (Ra) of 0.08±0.05µm. The reinforcement material selected in this study is graphite (micro-size, nano-size, and plate).

Table 1
The properties of the AA2017 substrate

Properties	Value
Composition	Al: 90.61%, O: 5.73%, Cu: 3.66%
Hardness	135HV
Ultimate tensile strength	427MPa
Yield strength	276MPa
Shear Strength	262MPa

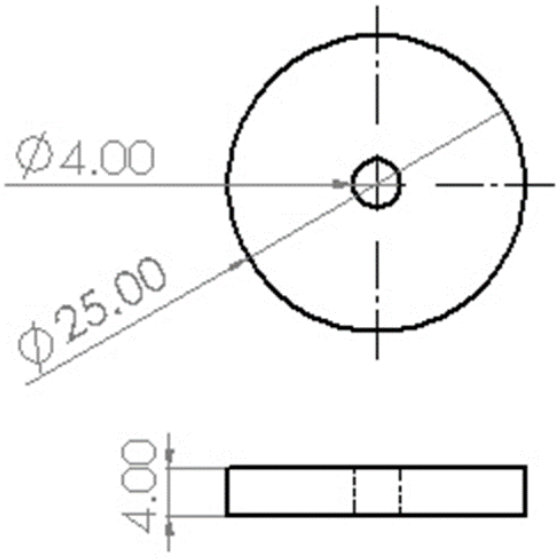

Fig. 1. The dimensions of the AA2017 substrate

2.2 Anodizing Process

The polished substrates were first cleaned by using an ultrasonic bath in ethanol for about 10 minutes before being dried and anodized. As mentioned in the previous section, there are three types of graphite source reinforcement used in this study: micro-sized, nano-sized, and graphite plate. For a standard datum, anodic oxide without graphite was also anodized. Table 2 shows the arrangement of the anode, cathode, and electrolyte used in this study.

Table 2
Arrangement of sample fabrication (anodized)

Sample name	Anode	Cathode	Electrolyte
AO	AA2017	SUS316L	20% H_2SO_4
AO micro	AA2017	SUS316L	20% H_2SO_4 + (graphite + ethanol)
AO nano	AA2017	SUS316L	20% H_2SO_4 + (graphite + ethanol)
AO plate	AA2017	Graphite plate	20% H_2SO_4

For sample AO micro and AO nano, the 1.0g/L graphite was first mixed with 20mL/L ethanol and stirred for 20 minutes at 250rpm before mixing with the sulphuric acid (H_2SO_4) for the anodizing process. With a DC power supply, the current was set to be constant throughout the anodizing process at 2A with fluctuating voltage at 15V maximum. Based on the previous preliminary study, the growth time was set to be 60 minutes in order to produce a fully covered oxide coating with this set-up condition. A magnetic stirrer with 250rpm speed was used to stir the electrolyte. The set-up

diagram for the anodizing is shown in Figure 2. The anodized sample was then rinsed with distilled water before being left to dry under ambient temperature.

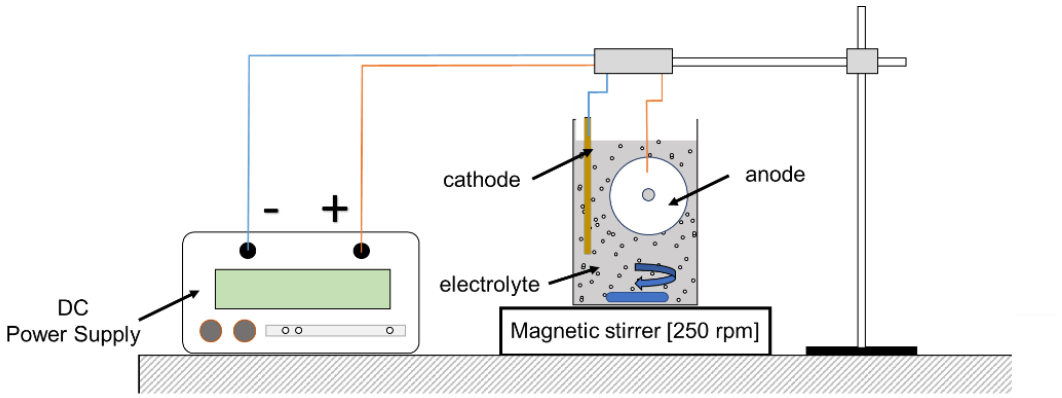

Fig. 2. Illustration of the anodizing set-up

2.3 Surface Analysis

The dried sample was first analyzed by using a 3D surface profilometer for its surface roughness analysis. Then, the surface's hardness was analyzed using Vicker's Micro-hardness tester at 0.25N load and 10 seconds of indentation duration by complying with the American Society for Testing and Materials (ASTM) E384. The illustration of indentation and its calculation is shown in Figure 3 and Eq. (1).

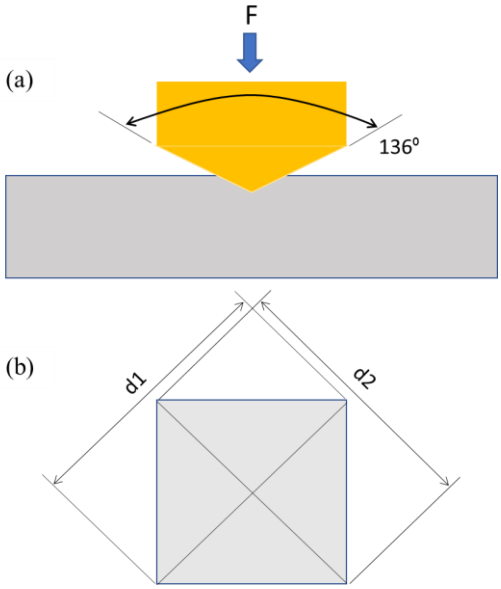

Fig. 3. Illustration of the Vicker's micro-hardness indentation for (a) indenter indenting the sample, and (b) indentation mark

$$\mathrm{HV} = \frac{2\mathrm{F}_{\sin\frac{136^\circ}{2}}}{\mathrm{d}^2}$$
$$\mathrm{HV} = 1.854\frac{\mathrm{F}}{\mathrm{d}^2} \quad (1)$$

where *F* is the applied load in *kgf, d* is the arithmetic mean of the two diagonals (*d1* and *d2* in mm), and *HV* is Vicker's micro-hardness.

The detailed surface condition was observed by using Scanning Electron Microscope (SEM), while the presence of graphite (Carbon) was observed by using Energy Dispersive X-ray Spectroscopy (EDS).

2.4 Tribological Analysis

Finally, the sample undergoes a dry sliding test using a ball-on-disc tribotester by obeying the ASTM G99. The testing parameter for the ball-on-disc test is shown in Table 3. The friction force was recorded continuously against the sliding time and later converted into the coefficient of friction (COF), as shown in Eq. (2). Meanwhile, the wear rate was calculated based on Archard Equation, as shown in Eq. (3). The schematic diagram of the ball-on-disc tribotester is shown in Figure 4. The sample (flat surface) will be placed horizontally and rotated. The ball will be then pressed on the rotating surface allowing the resistivity of the sliding motion (friction) to be determined.

Table 3
The testing parameters for the ball-on-disc test

Parameters	
Samples	AO, AO micro, AO nano, AO plate
Counter surface material	Silicon nitride (Si_3N_4)
Counter surface size	8mm
Applied load	1N
Sliding speed	31.416mm/s
Wear track diameter	10mm
Rotation number	1000
Relative humidity	50%
Temperature	27ºC

$$F = \mu N \quad (2)$$

where *F* is the friction force (N), and *N* is the applied load (N).

$$\mathrm{k} = \frac{\mathrm{V_{total}}}{\mathrm{ND}} \quad (3)$$

where the V_{total} is the total volume loss (mm^3), *N* is the applied load (N), and *D* is the sliding distance (m).

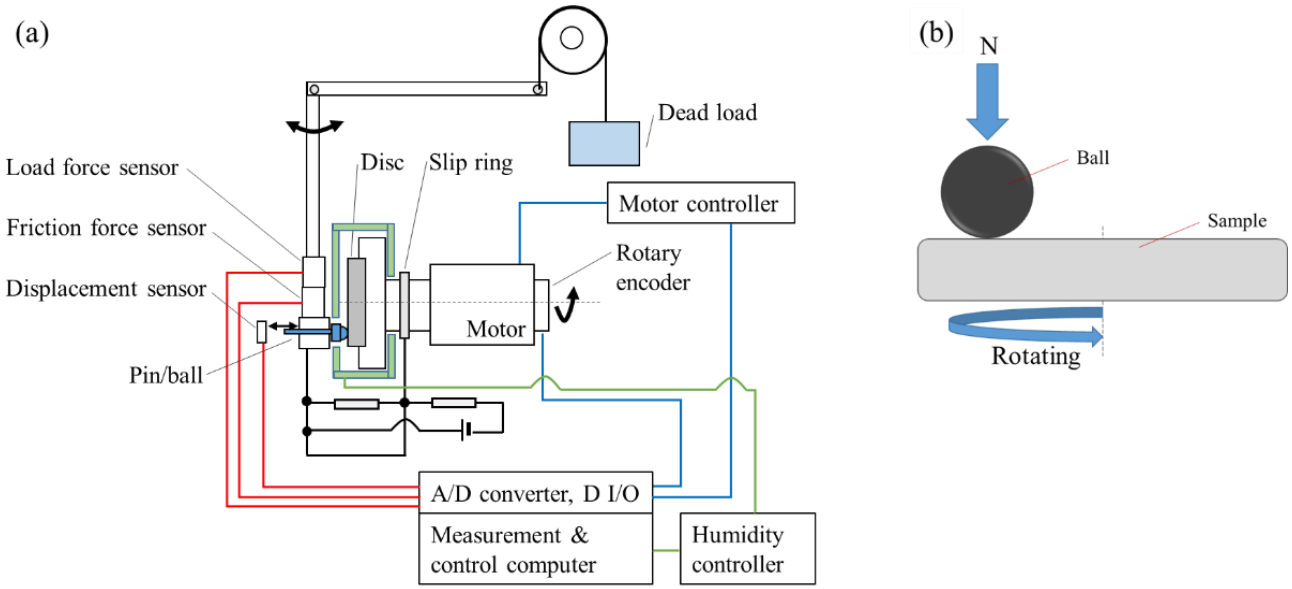

Fig. 4. Illustration of (a) The schematic diagram of the ball-on-ball tribotester (b) A close-up image of the ball and disc

3. Results

3.1 Surface Performance

The surface roughness and hardness were compared with the bare AA2017 substrate (un-anodized), along with samples AO, AO micro, AO nano, and AO plate. Figure 5 shows the images obtained from the 3D surface profilometer of the surfaces. The images were represented by pseudo color information where blue represents the low and red color represents the high region. The image area is 696173 μm^2 and was taken at four different areas on each sample. Figure 6 shows the comparison graph of the surface roughness and hardness for each surface.

Figure 5(a) to (e) shows the 3D surface profilometer for all samples, including the bare AA2017 substrate. Except for the bare substrate, all anodized surface has higher surface roughness and are presented with pores and crates. It was discussed that the formation of the oxide layer by anodizing is through the formation of a non-porous barrier layer followed by a porous structure. The oxide layer formation happens when the anode cation Al^{3+} (in this study: AA2017) moves to the interface between the oxidized layer zone and the electrolytes, where O^{2-} anions are transported from the electrolyte to the interface between the AA2017 and the oxidized layer zone [3,29]. As a result, the molten oxides and gas bubbles are released out of the outlet channels due to the electrical discharge process that sparks during high-voltage electrolytic oxidation that creates pores.

The AO nano has the lowest surface roughness compared to other anodizing surfaces. Here, it can be said that the reinforcement size plays a crucial role in the adsorption of the reinforcement in the coating. This idea can be supported by the previous researcher, who found that the nano-sized graphite particles have the least porosity and are able to provide a smooth surface compared to micro-sized graphite. It was discussed that the incorporation of nano graphite able to seal the pores and increase the densification of the coating [30,31]. Interestingly, the AO plate has the highest surface roughness among others. Although the pores are relatively smaller compared to the AO surface, the AO plate surface has many uneven peaks throughout the surface. To clarify this finding, further analyses on SEM were conducted and will be discussed later.

With the presence of an oxide coating, the surface's hardness shows an increment compared to the bare AA2017 surface. From Figure 6, it can be seen that the hardness also increased as the

reinforcement was added to the oxide coating. Among all, AO nano has the highest hardness, followed by AO micro and AO plate sample. The densification of nano-sized graphite into the AO nano surface was believed to be the critical factor for its high hardness compared to the other surface. Regardless of its high surface roughness, the hardness of the AO plate is almost the same as the AO micro. To understand this phenomenon more, an SEM image compilation of these surfaces is shown in Figure 7.

The SEM image shown in Figure 7 shows samples at ×500 and ×1500 magnification. From the images, micro and nano-cracks are visible in AO and AO plate samples (as shown in Figure 7(b) and Figure 7(h)), indicating surface defects. In contrast, the AO micro and nano samples have no clear and visible cracks. The EDS analysis (in Table 4) conducted on marked red points indicates the presence of carbon elements on the surface. From the table, it can be confirmed that all three AO micro, nano, and plate are presented with carbon but at different conditions and sizes. Interestingly, it can be seen from the SEM images that carbon elements (in this case graphite) are embedded inside the pores for AO micro and AO nano samples; meanwhile, the carbon element in the AO plate lies on top of the surface due to its relatively large size. It was discussed that the graphite particles underwent self-diffusion during the process, moving from areas with greater concentrations of electrolytes containing graphite to areas with lower concentrations close to the anode surface. In addition, the electrophoresis effect moved the graphite particles to the anode surface due to the electrical force between the anodizing cells. Therefore, upon the oxide film's solidification, the graphite particles that had adsorbed to the film surface would be integrated [3,8,31,32].

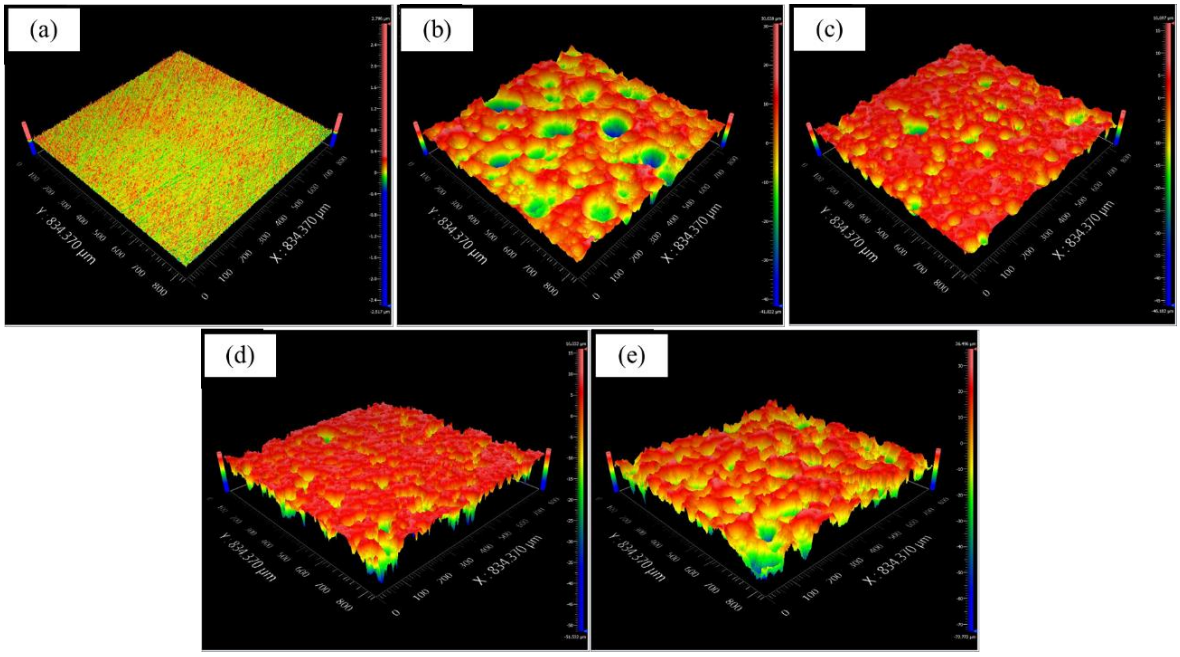

Fig. 5. Surface roughness image observed from the 3D surface profiler for (a) Bare AA2017 (b) AO (c) AO micro (d) AO nano (e) AO plate

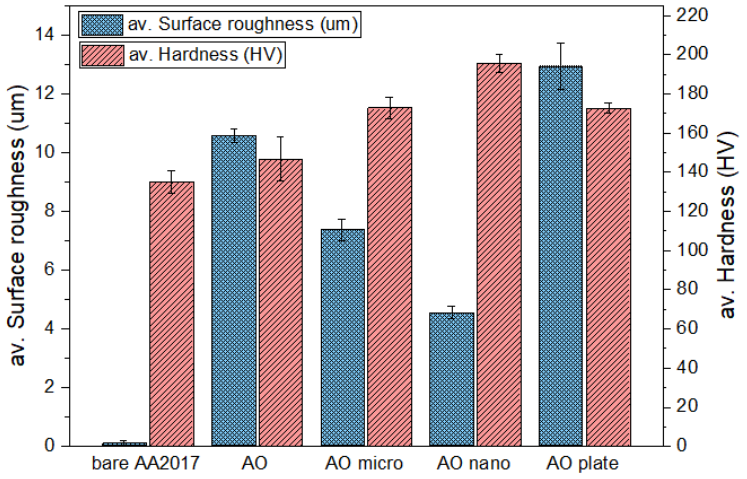

Fig. 6. Comparison graph for average surface roughness (left axis) and average hardness (right axis)

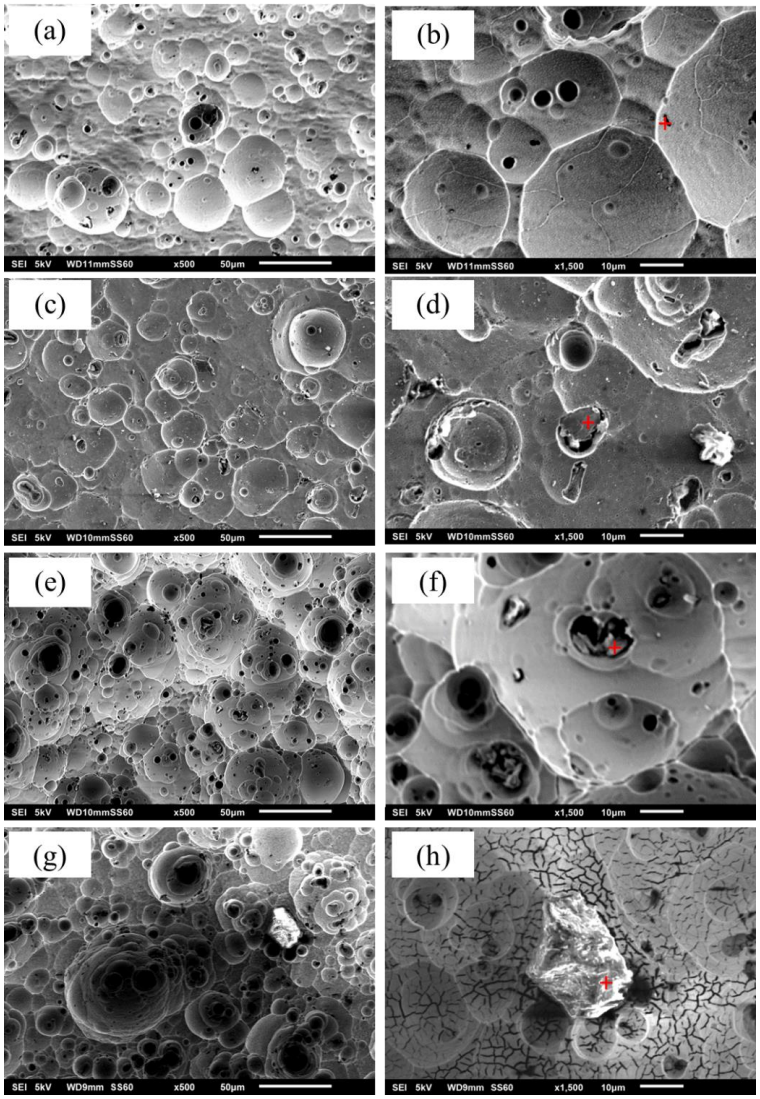

Fig. 7. SEM images of samples (a) At x500 AO (b) At x1500 AO (c) At x500 AO micro (d) At x1500 AO micro (e) At x500 AO nano (f) At x1500 AO nano (g) At x500 AO plate (h) At x1500 AO plate

Table 4
EDS analysis on the spectrum

Sample	Element content
AO – Figure 7(b)	C: 00.00%, 0: 48.51%, Al: 50.47%, Si: 01.02%
AO micro – Figure 7(d)	C: 96.58%, 0: 01.00%, Al: 01.97%, Si: 00.45%
AO nano – Figure 7 (f)	C: 83.08%, 0: 12.57%, Al: 04.35%, Si: 00.00%
AO plate – Figure 7(h)	C: 98.32%, 0: 00.70%, Al: 00.00%, Si: 00.98%

Besides that, mechanical entrapment was another way of embedment of graphite particles into the oxide coating. This trapping may take place in one of two ways: either inside the pores or during the oxide film's solidification. A comparable process for the PTFE particles inside the anodic oxide coating was presented by Chen *et al.,* [29]. Additionally, they claimed that some big particles had rushed into the film's larger holes while small particles had entered nano-sized pores. Meanwhile, other researchers claimed that smaller graphite particles are easier to adsorb into the film and are stuck in the pore compared to bigger graphite particles [31]. Due to the oxide film's size restriction, there is some possibility that large particles could only partially embed.

Xiang *et al.,* [33] utilized a graphite plate as its carbon reinforcement source for nickel plating on the SS304 substrate. They declared that graphene was exfoliated from the graphite plate and embedded on the surface along with the nickel. From the observed images, graphene lays on the coating surface with some nickel particles spread on top. It can also be seen that the graphene layers are in a large surface area. However, there are some defects presented that they clarified to occur due to the electrochemical stripping and deposition process. Thus, by comparing with this study, the graphene exfoliated indeed has a large surface area. Still, it fails to lay flat on the surface but agglomerated and folded on top of the oxide surface.

3.2 Friction and Wear Performance

The ball-on-disc tribotester findings are represented by a continuous graph against the number of rotations, as shown in Figure 8.

From the graph presented in Figure 8, it can be seen that the AO nano and AO plate show relatively the same pattern and value; meanwhile, the AO micro shows almost the same pattern as the AO in the beginning. Since the behavior changes throughout as the no. of rotations increases, the analysis can be divided into two phases (Phase I and II).

In phase I, it can be seen that the coefficient of friction (COF) for AO starts low and increases as the number of rotations increases; meanwhile, the other sample starts with a relatively high COF and decreases as the number of rotations increases. Unlike the AO nano and AO plate, the COF for AO micro decreased at the beginning and started to increase as it reached the 50^{th} rotation. Then, after reaching almost 0.6, the COF stays within that value and decreases as it reaches the 300^{th} rotation. Interestingly, the COF kept decreasing as the rotations increased, producing lower COF than the AO nano and AO micro in Phase II.

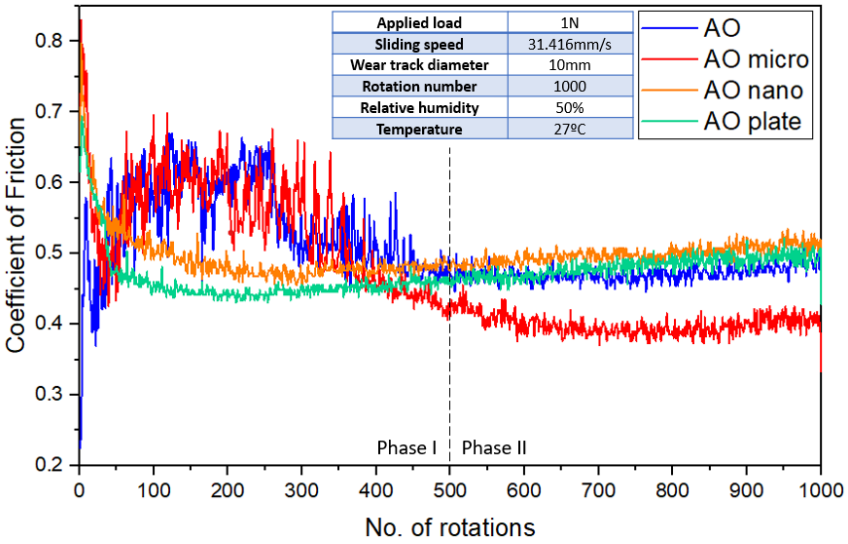

Fig. 8. Coefficient of friction graph obtained from the ball-on-disc tribotester

The COF shows a lesser noise with a relatively stable value in Phase II, where the average COF can be obtained within this phase. The calculated average COF was then compared and plotted along with the calculated wear rate, as shown in Figure 9.

The data plotted in Figure 9 shows a different distribution pattern between the COF and wear rate. The COF for all samples presents almost the same value at around 0.4 – 0.5 with its standard deviation bar presented. Thus, it can be said that the addition of reinforcement on the anodic oxide coating did not improve its COF performance. Among all, AO micro presents the lowest COF of 0.40. On the other hand, variations in wear rate distribution can be observed from the same graph. It can be seen that AO micro presents the lowest wear rate at 1.25×10^{-5} mm^3/Nm, followed by AO plate, AO nano, and AO samples at 2.21×10^{-5}, 3.24×10^{-5}, and 3.42×10^{-5} mm^3/Nm respectively.

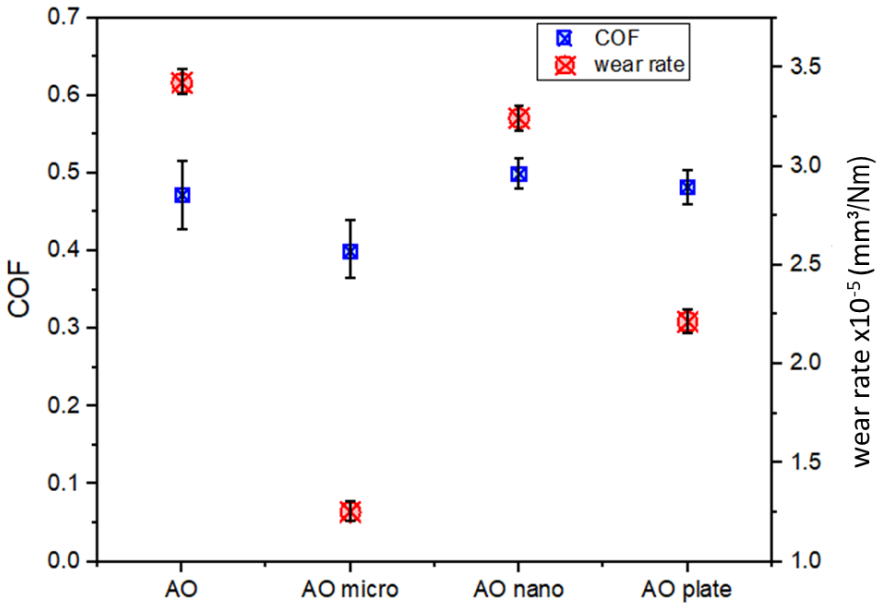

Fig. 9. Comparison of COF and wear rate for all samples

Although it has been discussed earlier that the size of particles plays a vital role in improving the surface quality, which shows the AO nano provides the best, the finding did not correlate with the tribological performance. Here, it can be observed that the AO micro provides the lowest COF and wear rate surpassing the others. It was explained by previous research that these four key factors—the hardness of the coating to the substrate, the hardness of the surface, the hardness of the coating's thickness, and the size and hardness of the debris—can be used to define contacts between two surfaces that are either one or both coated [34]. As a result of the link between the characteristics mentioned above, various contact circumstances that specific contact mechanisms may characterize were created.

Similar research focusing on DLC coatings with varying surface roughness was conducted by Suzuki *et al.,* [35]. They discovered that the various surface roughness tests had no discernible impact on the coefficient of friction on surfaces that were lubricated. However, when they examined the wear analyses, they discovered that varying surface roughness results in varying wear rates, which in turn results in varying wear processes. It was also discussed and agreed that the dominant wear mechanisms for coating may vary from adhesion to chip-flake formation and fragmentation depending on the surface roughness of the coating [36]. Figure 10 shows proof of the discussed idea on the wear track of this study which correlates with the previous argument.

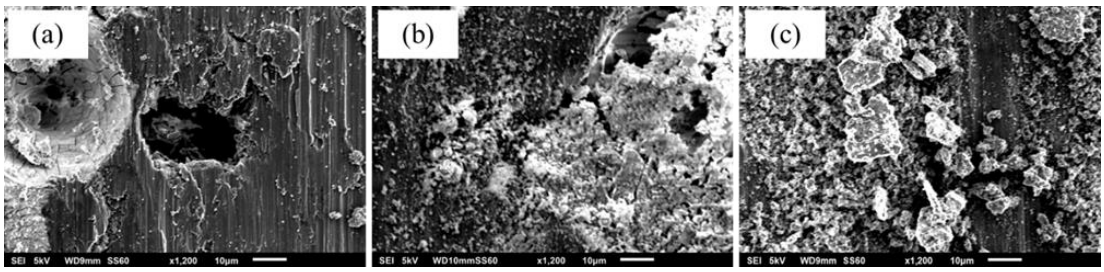

Fig. 10. Comparison of worn surface of (a) AO micro (b) AO nano (c) AO plate

4. Conclusions

The present study mainly focused on the surface refinement of anodic oxide coating reinforced with the different conditions of carbon-based material, in this case, graphite particles at micro-sized, nano-sized, and graphite plates. The reinforcement was introduced during the anodizing process and interestingly gave various mechanical and tribological performances. Hence, it can be concluded that

i. All anodic oxide coating successfully increased the surface hardness with AO nano has the highest hardness of 195.85HV due to its smoother surface. The surface of AO nano samples was observed to be free from micro-cracks. The AO plate has the highest surface roughness among all samples due to the micro-cracks on its surface and the pores formed during the anodizing process.
ii. Tribologically, although there is not much difference in the COF between those samples, AO micro presents the lowest COF and wear rate of 0.4 and 1.25×10^{-5} mm^3/Nm, respectively. The worn surface shows different traces of wear debris, indicating different dominant wear occurs between those surfaces.

Acknowledgment
This research was funded by Universiti Teknologi Malaysia, Malaysia, through the Post-Doctoral Fellowship Scheme (PDRU Grant number: Q.K130000.21A2.05E39) and JICA Fund Program 2021 under the Technical Cooperation Project for Enhancement of Malaysia-Japan International Institute

of Technology: R.K130000.7343.4B694. The authors also acknowledge the support provided by the Tribology and Precision Machining i-Kohza for the facilities and equipment provided.

References

[1] Abd El-Hameed, Afaf M., and Y. A. Abdel-Aziz. "Aluminium Alloys in Space Applications: A Short Report." *Journal of Advanced Research in Applied Sciences and Engineering Technology* 22, no. 1 (2021): 1-7. https://doi.org/10.37934/araset.22.1.17

[2] Gorokh, G. G., M. I. Pashechko, J. T. Borc, A. A. Lozovenko, I. A. Kashko, and A. I. Latos. "Matrix coatings based on anodic alumina with carbon nanostructures in the pores." *Applied surface science* 433 (2018): 829-835. https://doi.org/10.1016/j.apsusc.2017.10.117

[3] Mohamad, Syazwani, Shahira Liza, and Yazid Yaakob. "Strengthening of the mechanical and tribological properties of composite oxide film formed on aluminum alloy with the addition of graphite." *Surface and Coatings Technology* 403 (2020): 126435. https://doi.org/10.1016/j.surfcoat.2020.126435

[4] Gasco-Owens, A., D. Veys-Renaux, V. Cartigny, and E. Rocca. "Large-pores anodizing of 5657 aluminum alloy in phosphoric acid: An in-situ electrochemical study." *Electrochimica Acta* 382 (2021): 138303. https://doi.org/10.1016/j.electacta.2021.138303

[5] Bruera, Florencia A., Gustavo R. Kramer, María L. Vera, and Alicia E. Ares. "Low-cost nanostructured coating of anodic aluminium oxide synthesized in sulphuric acid as electrolyte." *Coatings* 11, no. 3 (2021): 309. https://doi.org/10.3390/coatings11030309

[6] Mat Tahir, Noor Ayuma, Shahira Liza, Kanao Fukuda, Syazwani Mohamad, Mohd Zakir Fathi Hashimi, Mohd Saifulnizam Mohd Yunus, Yazid Yaakob, and Intan Sharhida Othman. "Surface and tribological properties of oxide films on aluminium alloy through fly-ash reinforcement." *Coatings* 12, no. 2 (2022): 256. https://doi.org/10.3390/coatings12020256

[7] Chen, Luanxia, Zhanqiang Liu, Bing Wang, Qinghua Song, Yi Wan, and Long Chen. "Surface characterization and tribological performance of anodizing micro-textured aluminum-silicon alloys." *Materials* 12, no. 11 (2019): 1862. https://doi.org/10.3390/ma12111862

[8] Wang, Bin, Shengguan Qu, and Xiaoqiang Li. "Preparation and anodizing of SiCp/Al composites with relatively high fraction of SiCp." *Scanning* 2018 (2018). https://doi.org/10.1155/2018/8945729

[9] He, Chunlin, Qi Zhou, Jiangtao Liu, Xuewen Geng, and Qingkui Cai. "Effect of size of reinforcement on thickness of anodized coatings on SiC/Al matrix composites." *Materials Letters* 62, no. 16 (2008): 2441-2443. https://doi.org/10.1016/j.matlet.2007.12.016

[10] Lu, Xiaopeng, Carsten Blawert, Yuanding Huang, Henry Ovri, Mikhail L. Zheludkevich, and Karl Ulrich Kainer. "Plasma electrolytic oxidation coatings on Mg alloy with addition of SiO2 particles." *Electrochimica Acta* 187 (2016): 20-33. https://doi.org/10.1016/j.electacta.2015.11.033

[11] Abedini, Amin, Ali Asghar Ebrahimi Valmoozi, and Seyyed Salman Seyyed Afghahi. "Anodized graphite as an advanced substrate for electrodeposition of PbO2." *Materials Today Communications* 31 (2022): 103464. https://doi.org/10.1016/j.mtcomm.2022.103464

[12] Bhaskar, Sourabh, and Mukesh Kumar. "Effect of graphite particulates on sliding wear performance of hybrid AA2024 alloy composites." *Journal of Materials Engineering and Performance* 30 (2021): 3976-3989. https://doi.org/10.1007/s11665-021-05677-5

[13] Li, Zheng-yang, Zhen-bing Cai, Yuan Ding, Xue-Jun Cui, Zhong-bo Yang, and Min-hao Zhu. "Characterization of graphene oxide/ZrO2 composite coatings deposited on zirconium alloy by micro-arc oxidation." *Applied Surface Science* 506 (2020): 144928. https://doi.org/10.1016/j.apsusc.2019.144928

[14] Shang, Wei, Fang Wu, Yuanyuan Wang, Amin Rabiei Baboukani, Yuqing Wen, and Jiqiong Jiang. "Corrosion resistance of micro-arc oxidation/graphene oxide composite coatings on magnesium alloys." *Acs Omega* 5, no. 13 (2020): 7262-7270. https://doi.org/10.1021/acsomega.9b04060

[15] Cui, Lan-Yue, Shang-Dong Gao, Ping-Ping Li, Rong-Chang Zeng, Fen Zhang, Shuo-Qi Li, and En-Hou Han. "Corrosion resistance of a self-healing micro-arc oxidation/polymethyltrimethoxysilane composite coating on magnesium alloy AZ31." *Corrosion Science* 118 (2017): 84-95. https://doi.org/10.1016/j.corsci.2017.01.025

[16] Goyal, R. K., and M. Yadav. "The wear and friction behavior of novel polytetrafluoroethylene/expanded graphite nanocomposites for tribology application." *Journal of tribology* 136, no. 2 (2014). https://doi.org/10.1115/1.4025655

[17] Montazeri, M., C. Dehghanian, M. Shokouhfar, and A. Baradaran. "Investigation of the voltage and time effects on the formation of hydroxyapatite-containing titania prepared by plasma electrolytic oxidation on Ti–6Al–4V alloy and its corrosion behavior." *Applied Surface Science* 257, no. 16 (2011): 7268-7275. https://doi.org/10.1016/j.apsusc.2011.03.103

[18] Vahedi, Shaghayegh, Rouhollah Mehdinavaz Aghdam, Ali Hossein Rezayan, and Mahmoud Heydarzadeh Sohi. "Carbon nanotubes reinforced electrospun chitosan nanocomposite coating on anodized AZ31 magnesium alloy." *Journal of Ultrafine Grained and Nanostructured Materials* 53, no. 1 (2020): 71-77.
[19] Hwang, Myungwon, and Wonsub Chung. "Effects of a carbon nanotube additive on the corrosion-resistance and heat-dissipation properties of plasma electrolytic oxidation on AZ31 magnesium alloy." *Materials* 11, no. 12 (2018): 2438. https://doi.org/10.3390/ma11122438
[20] Sabouri, M., and SM Mousavi Khoei. "Plasma electrolytic oxidation in the presence of multiwall carbon nanotubes on aluminum substrate: morphological and corrosion studies." *Surface and Coatings Technology* 334 (2018): 543-555. https://doi.org/10.1016/j.surfcoat.2017.10.045
[21] Isaza M, Cesar A., Benjamín Zuluaga D, Juan S. Rudas, Hugo A. Estupiñán D, José M. Herrera R, and Juan M. Meza. "Mechanical and corrosion behavior of plasma electrolytic oxidation coatings on AZ31B Mg alloy reinforced with multiwalled carbon nanotubes." *Journal of Materials Engineering and Performance* 29 (2020): 1135-1145. https://doi.org/10.1007/s11665-020-04633-z
[22] Skoneczny, W., and M. Bara. "Aluminium oxide composite layers obtained by the electrochemical method in the presence of graphite." *Materials Science-Poland* 25, no. 4 (2007).
[23] Bagde, Pranay, Sanket Mehar, S. G. Sapate, and Avishkar Rathod. "Effect of graphite addition on tribological behaviour of plasma sprayed Cr2O3-TiO2 coating." *Materials Today: Proceedings* 56 (2022): 2365-2370. https://doi.org/10.1016/j.matpr.2021.12.166
[24] Bagde, Pranay, S. G. Sapate, R. K. Khatirkar, and Nitesh Vashishtha. "Friction and abrasive wear behaviour of Al2O3-13TiO2 and Al2O3-13TiO2+ Ni Graphite coatings." *Tribology International* 121 (2018): 353-372. https://doi.org/10.1016/j.triboint.2018.01.067
[25] Pezzato, L., V. Angelini, K. Brunelli, C. Martini, and M. Dabalà. "Tribological and corrosion behavior of PEO coatings with graphite nanoparticles on AZ91 and AZ80 magnesium alloys." *Transactions of Nonferrous Metals Society of China* 28, no. 2 (2018): 259-272. https://doi.org/10.1016/S1003-6326(18)64659-X
[26] Zuo, You, Tianlu Li, Peihang Yu, Zicong Zhao, Xiaoyi Chen, You Zhang, and Fei Chen. "Effect of graphene oxide additive on tribocorrosion behavior of MAO coatings prepared on Ti6Al4V alloy." *Applied Surface Science* 480 (2019): 26-34. https://doi.org/10.1016/j.apsusc.2019.02.065
[27] Zhang, Yulin, Fei Chen, You Zhang, and Cuiwei Du. "Influence of graphene oxide additive on the tribological and electrochemical corrosion properties of a PEO coating prepared on AZ31 magnesium alloy." *Tribology International* 146 (2020): 106135. https://doi.org/10.1016/j.triboint.2019.106135
[28] Zhao, Jingmao, Xiong Xie, and Chen Zhang. "Effect of the graphene oxide additive on the corrosion resistance of the plasma electrolytic oxidation coating of the AZ31 magnesium alloy." *Corrosion Science* 114 (2017): 146-155. https://doi.org/10.1016/j.corsci.2016.11.007
[29] Chen, Suiyuan, Chen Kang, Jing Wang, Changsheng Liu, and Kai Sun. "Synthesis of anodizing composite films containing superfine Al2O3 and PTFE particles on Al alloys." *Applied Surface Science* 256, no. 22 (2010): 6518-6525. https://doi.org/10.1016/j.apsusc.2010.04.040
[30] Tonelli, Lavinia, Luca Pezzato, Paolo Dolcet, Manuele Dabalà, and Carla Martini. "Effects of graphite nano-particle additions on dry sliding behaviour of plasma-electrolytic-oxidation-treated EV31A magnesium alloy against steel in air." *Wear* 404 (2018): 122-132. https://doi.org/10.1016/j.wear.2018.03.012
[31] Arun, S., S. Hariprasad, A. Saikiran, B. Ravisankar, E. V. Parfenov, V. R. Mukaeva, and N. Rameshbabu. "The effect of graphite particle size on the corrosion and wear behaviour of the PEO-EPD coating fabricated on commercially pure zirconium." *Surface and Coatings Technology* 363 (2019): 301-313. https://doi.org/10.1016/j.surfcoat.2019.02.033
[32] Lv, Guo-Hua, Huan Chen, Wei-Chao Gu, Wen-Ran Feng, Li Li, Er-Wu Niu, Xian-Hui Zhang, and Si-Ze Yang. "Effects of graphite additives in electrolytes on the microstructure and corrosion resistance of Alumina PEO coatings." *Current Applied Physics* 9, no. 2 (2009): 324-328. https://doi.org/10.1016/j.cap.2008.03.001
[33] Xiang, Li, Qianqian Shen, Yu Zhang, Wei Bai, and Chaoyin Nie. "One-step electrodeposited Ni-graphene composite coating with excellent tribological properties." *Surface and Coatings Technology* 373 (2019): 38-46. https://doi.org/10.1016/j.surfcoat.2019.05.074
[34] Holmberg, Kenneth, Allan Matthews, and Helena Ronkainen. "Coatings tribology—contact mechanisms and surface design." *Tribology international* 31, no. 1-3 (1998): 107-120. https://doi.org/10.1016/S0301-679X(98)00013-9
[35] Suzuki, M., T. Ohana, and A. Tanaka. "Tribological properties of DLC films with different hydrogen contents in water environment." *Diamond and related materials* 13, no. 11-12 (2004): 2216-2220. https://doi.org/10.1016/j.diamond.2004.06.023
[36] Singh, R. K., Z. H. Xie, A. Bendavid, P. J. Martin, Paul Munroe, and Mark Hoffman. "Effect of substrate roughness on the contact damage of DLC coatings." *Diamond and related materials* 17, no. 6 (2008): 975-979.https://doi.org/10.1016/j.diamond.2008.02.037